DOI: 10.13009/EUCASS2023-090
Aerospace Europe Conference 2023 – 10TH EUCASS – 9TH CEAS

Sandwich hybrid structural component for tilt rotor aircraft

Giuseppe Mantegna[⋆†], *Carmelo Rosario Vindigni*[⋆], *Davide Tumino*[⋆], *Calogero Orlando*[⋆], *Andrea Alaimo*[⋆]
[⋆]*Kore University of Enna, Faculty of Engineering and Architecture*
Cittadella Universitaria, 94100 Enna, Italy
giuseppe.mantegna@unikore.it · carmelorosario.vindigni@unikore.it · davide.tumino@unikore.it ·
calogero.orlando@unikore.it · andrea.alaimo@unikore.it
[†]Corresponding author

Abstract

Sandwich structures have been increasingly used due to their high strength-to-weight ratio and bending and buckling resistance. Today, it is possible to create topology-optimised structures with complex shapes using lattice structures through Additive Manufacturing technologies, avoiding the difficulties in core-sheets adhesion in sandwich structures. In this paper, a 3D numerical model is proposed to assess the mechanical properties of hybrid lattice structures. A comparison between the overall response of a control surface of a tiltrotor aircraft with different cores for its sandwich panels will be studied. Specifically, two strut lattice cores and a conventional honeycomb lattice core are considered as options for the asymmetric sandwich panels.

1. Introduction

Tilt rotors are hybrid aircraft capable of shifting between vertical take-off and landing (VTOL), hovering in mid-air, and efficient forward flight thanks to their rotors which can rotate around the pitch aircraft axis and assume a vertical or a horizontal position.
The versatility of these aircraft makes them well-suited for a range of applications, including aerial transportation, search and rescue operations, military missions, and to reduce air and ground congestion. In order to reduce fuel consumption and emissions, while maximizing the payload ratio and maintaining structural integrity and safety, engineers and designers constantly seek new lightweight structures. Sandwich structures, multi-layered structures formed by high-strength outer layers (faces) separated by a thick low-density inner layer (core)[1] , have been increasingly used due to their high strength-to-weight ratio and their bending and buckling resistance[2,3] . According to Castanie et al.[4] two main types of sandwich structures can be defined: Symmetrical and Asymmetrical sandwiches. The former is particularly suitable for pressurized structures or those exposed to aerodynamic loads. Conversely, the latter is commonly employed in non-pressurized and moderately loaded structures and can alleviate the joint difficulties of different panels.
With the advent of Additive Manufacturing (AM) technologies, new possibilities in materials and core topologies are available, enhancing their performances and characteristics of sandwich structures. By leveraging the freedom design provided by AM, it is possible to fabricate complex lattice or cellular structures within the core layer, enhancing its energy absorption capacity, thermal insulation properties, and overall weight reduction. Wicks and Hutchinson[5] have shown improved performances against bending and compression loads of truss core sandwich panels. Furthermore, truss core sandwich panels have demonstrated their utility in heat transfer applications and can be exploited also for structural anti-icing systems[6] . These panels leverage the truss-like internal structures within the core layer to efficiently distribute heat and prevent the formation of ice on the outer surfaces. In a study conducted by Kohsaka et al.[7] , the vibration characteristics of sandwich structures with a lattice beam Body-Cantered Cube (BCC) core were investigated. The findings of the study revealed that when compared to a brick core, the sandwich structures with a BCC core consistently exhibited higher maximum frequencies, thereby enhancing the vibration response. The BCC lattice structure was also investigated in Tancogne and Mohr[8] . A monotonic increase in the stress-strain compression curve, followed by a plateau region before the densification stage, suggests the application of these structures as energy absorption systems for crushing applications.
The full capabilities of AM technologies can be achieved with metamaterials, which are structured materials possessing distinct mechanical properties designed for specific purposes and optimized across various regions of the structure. One approach to achieve this optimization is through the design of topology-optimized structures using periodic lattice cells, where cell types, dimensions, or relative volume fractions can be varied[9] . By employing this methodology, structures

DOI: 10.13009/EUCASS2023-090

with graded or separate regions can be manufactured in a single process, significantly reducing the design-to-production time and enabling rapid iteration and design optimization.
The mechanical properties of cellular materials are influenced by several factors, including the relative density, the base material, and the architecture of the unit cell. These elements collectively determine the response of the structure when subjected to external macroscopic loads which can deform the cell by a combination of bending, twisting, and stretching modes, thus significantly influencing its overall macroscopic behaviour[10] . In their work, Al-Ketan et al. compare the properties of strut-based lattice cells with triply periodic minimal surfaces cell structures like the skeletal-TPMS and sheet-TPMS. While strut-based cells like the Kelvin and Gibson-Ashby structures exhibit mixed stretch/bending mode deformation, a bending-dominated and a stretching-dominated behaviour was observed for the skeletal-TPMS and for the sheet-TPMS, respectively. In a recent work[11] , Tumino et al. explored the mechanical properties of waved-strut lattice cells highlighting an increase in the longitudinal uniaxial modulus and a negligible effect on the transverse moduli. Several studies are present in the literature to estimate the mechanical properties of lattice cells[12,13] .To reduce the computational costs of numerical analyses, a modified-beam approach which uses the concept of stiff beam-length is proposed in the work of Tumino et al.[14] .
The objective of this research paper is to evaluate the mechanical properties of hybrid lattice structures through numerical analyses. Specifically, a three-dimensional (3D) model is used to capture the essential behaviour of a BCC and a sine-Waved Body Centered Cubic (WBCC) lattice structures. The homogenised mechanical properties are used in comparative study of the overall response of a control surface of a tiltrotor aircraft. Specifically, the focus is on the asymmetric sandwich panels of the control surface, which employ the two mentioned strut lattice structures and a classic honeycomb lattice core to explore the capabilities of these new emerging structures.

2. Lattice Cells Homogenisation

2.1 Body Centered Cubic & Waved Body Centered Cubic Lattice Cells

At first, the mechanical properties of the single BCC and WBCC unit cells are determined. The methodology proposed considers a full 3D Finite Element Analysis in the commercial software Ansys; given the periodic nature of the unit element, significant attention is dedicated to establishing accurate boundary conditions. Specifically, a custom routine was developed using Ansys Parametric Design Language (APDL) to enforce double periodicity conditions.
Figure 1 depicts the Body Centered Cubic & sine-Waved Body Centered Cubic Lattice Cells considered for the numerical analysis. A cell length $L = 10\ mm$ is chosen for both the BCC and WBCC cells, while the strut waviness of the WBCC cell is described through a sine function with a period of $\sqrt{3}L$:

$$\psi = a \sin\left(\frac{2\pi\xi}{\sqrt{3}L}\right) \tag{1}$$

Indeed, the BCC cell can be seen as a special case of a WBCC cell with amplitude $a = 0\ mm$.
In order to compare the mechanical properties of the two cells, the same specific density, defined as the ratio between the volume of the cell and the volume of the box enclosing the cell itself, is selected: $\rho^* = V_c/V_b = 0.094$, while the other geometric parameters are accordingly selected in order to guarantee the desired density.

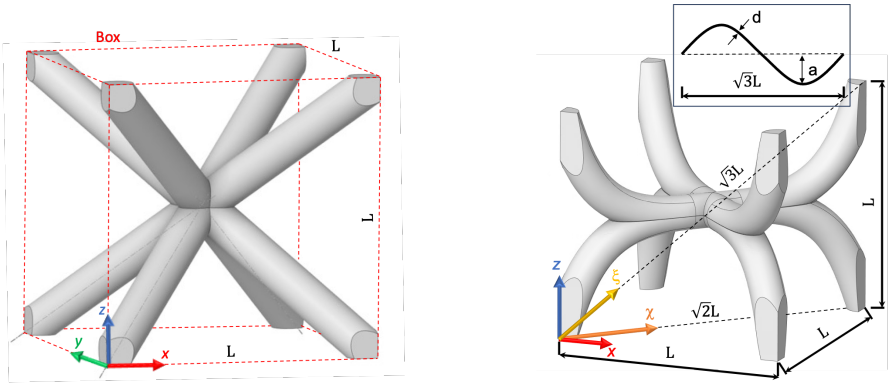

(a) (b)

Figure 1: Strut lattice cells. a. BCC lattice, strut diameter $d = 1.4\ mm$. b. WBCC lattice, $d = 1.5\ mm$, $a = 2.0\ mm$

DOI: 10.13009/EUCASS2023-090

A standard aluminium alloy is used as the base material for the two cells: $E = 71.0\ GPa, \nu = 0.33$.
As mentioned, specific periodicity conditions must be ensured due to the periodic nature of the cells. To this end, an ad-hoc routine was developed in Ansys Parametric Design Language (APDL) to impose double periodicity conditions along the selected directions through constraints equations pairing the displacements of the nodes in two opposite faces:

$$\begin{cases} u_{i_{x=0}} - u_{i_{x=L}} = u_{p_{x=0}} - u_{p_{x=L}} \\ v_{i_{x=0}} - v_{i_{x=L}} = v_{p_{x=0}} - v_{p_{x=L}} \\ w_{i_{x=0}} - w_{i_{x=L}} = w_{p_{x=0}} - w_{p_{x=L}} \end{cases} \tag{2}$$

where:
u, v, w are the displacements along the x, y, z-directions. $i_{x=0}$ and $i_{x=L}$ are the generic i^{th} node couple sharing the same relative position in the opposite faces, respectively; while $p_{x=0}$ & $p_{x=L}$ are two pilot nodes properly selected in the two faces.
Equation 2 refers to the periodicity conditions along the x-direction. In a similar way, it is possible to enforce the periodicity conditions along the y and z-direction. Since each node must have a paired node on the opposite face, only $1/8$ of the cell is first created and meshed, as shown in Figure 2a, to be subsequently mirrored, thus ensuring the correspondence of the nodes in the external faces of the lattice cells.

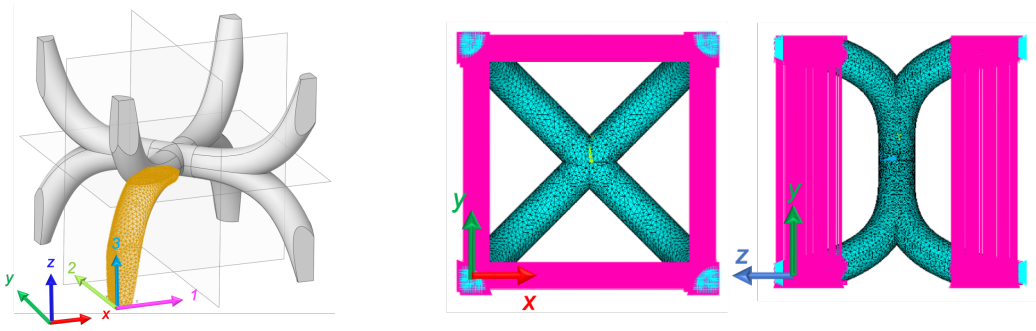

(a) (b)

Figure 2: a. Mirroring of one-eighth of WBCC strut. b. Graphical representation of constrain equations in x, y -direction.

The mechanical properties of the single unit cell are derived through a compression and shear test simulation. In addition to the double periodicity conditions previously described, the 3D model imposes specific displacement conditions as boundary conditions.
For the compression test, a displacement along the z-direction is applied to the upper surface ($z = L: \ w = -1\ mm$), while the respective displacement of the bottom surface is constrained ($z = 0: \ w = 0\ mm$). In contrast, the shear test considers an imposed displacement applied along the x direction on the upper face ($z = L: \ u = 1\ mm$), while the bottom surface has the relative displacements constrained ($z = 0: \ u = 0\ mm, \ w = 0\ mm$).
The homogenised orthotropic mechanical properties of the BCC and WBCC lattice cells are reported in Table 1.

Table 1: Homogenised mechanical properties Body-Centered Cubic and Waved-Body-Centered Cubic lattice cells.

	BCC	WBCC	
E_1	1.11E+08	1.61E+08	[Pa]
E_2	1.11E+08	1.61E+08	[Pa]
E_3	1.11E+08	1.11E+09	[Pa]
ν_{12}	0.481	0.824	
ν_{23}	0.481	0.074	
ν_{13}	0.481	0.074	
G_{12}	9.08E+08	8.51E+08	[Pa]
G_{23}	9.08E+08	9.26E+07	[Pa]
G_{13}	9.08E+08	9.26E+07	[Pa]

DOI: 10.13009/EUCASS2023-090

2.2 Honeycomb Lattice Cell

Finally, the mechanical properties of a honeycomb, with Hexagonal (Hex) unit cell reported in Figure 3, are evaluated. Similarly to the previous cases, a specific density $\rho^* = 0.094$ is selected, while the base of the enclosing box was selected so that $a * b = L^2$, leading to a cell length $l = 4.38\ mm$ and a thickness $t = 0.29\ mm$. The homogenised mechanical properties, retrieved analitically from the work of Kumar et al.[15] and Gibson and Ashby[16] , are: $E_1 =$ 4.63E+07 [Pa], $E_2 =$ 4.68E+07 [Pa], $E_3 =$ 7.20E+09 [Pa], $G_{12} =$ 2.81E+07 [Pa], $G_{23} =$ 1.52E+09 [Pa], $G_{13} =$ 1.02E+09 [Pa], $\nu_{12} = 0.99$.

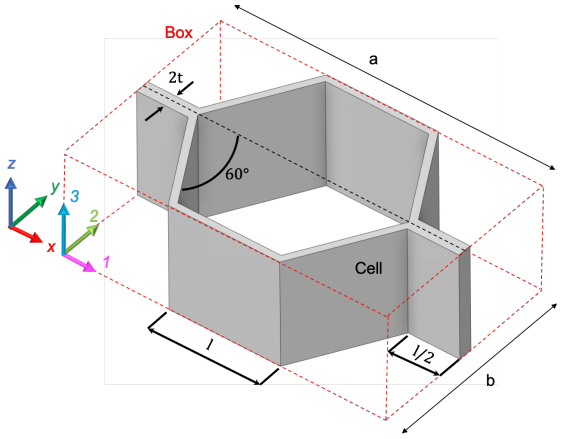

$$E_1 = \frac{4}{\sqrt{3}} E_s \frac{\left(\frac{t}{l}\right)}{\left[3 + \left(\frac{l}{t}\right)^2\right]} \qquad G_{12} = \frac{4\sqrt{3}}{5} E_s \left(\frac{t}{l}\right)^3$$

$$E_2 = 4\sqrt{3} E_s \frac{\left(\frac{t}{l}\right)}{\left[1 + 3\left(\frac{l}{t}\right)^2\right]} \qquad G_{23} = \frac{\sqrt{3}}{2}\left(\frac{t}{l}\right) G_s$$

$$E_3 = \frac{8}{3\sqrt{3}}\left(\frac{t}{l}\right) E_s \qquad G_{13} = \frac{1}{\sqrt{3}}\left(\frac{t}{l}\right) G_s$$

$$\nu_{12} = 1 - \frac{2}{3 + \left(\frac{t}{l}\right)^2} \qquad \nu_{31} = \nu_{32} = \nu_{bulk}$$

Figure 3: Honeycomb Cell, $l = 4.38mm$, $t = 0.29mm$.

From the homogenised mechanical properties retrieved, it is interesting noticing the Hex and WBCC cells have an orthotropic behaviour. At the same time, the BCC properties are equivalent in the three cartesian directions despite the cell not being isotropic in all directions.

3. New-generation Tiltrotor Control Surface

The control surface of a new-generation civil tiltrotor, reported in Figure 4, is considered in this study. Specifically, the upper and lower composite skins are reinforced with asymmetric sandwich panels, whose schematic representation in illustrated in Figure 5a, with the homogenised core properties previously exhamined.

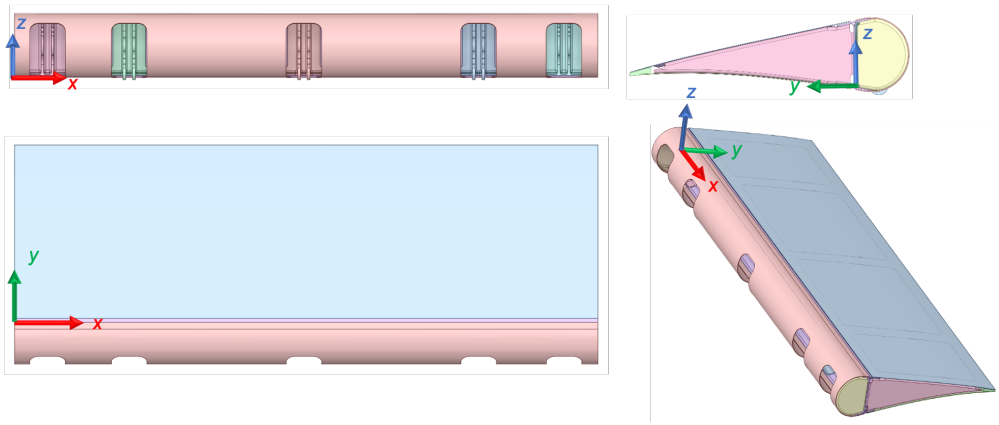

Figure 4: New-generation tiltrotor control surface. Front, Top, Lateral and Isometric view.

Furthermore, due to the instrinsic geometry orthotropy of the WBCC cell, a second configuration, namely WBCC2, will be considered. The WBCC is rotated so that the cell 3^{rd} axis is aligned with the global y-direction of the structure. The whole structure is modelled with 2D surfaces. The composite parts, namely the upper, lower and leading edge skins and the main spar, are modelled through the Ansys Composite Pre/Post (ACP) module. The composite laminates use epoxy-carbon woven prepreg plies whose mechanical properties are: $E_1 = E_2 =$ 6.13E+10 Pa, $E_3 =$ 6.90E+09 Pa, $\nu_{12} = 0.04$, $\nu_{23} = \nu_{13} = 0.3$, $G_{12} =$ 3.30E+09 Pa and $G_{23} = G_{13} =$ 2.70E+09 Pa. The main spar was modelled

DOI: 10.13009/EUCASS2023-090

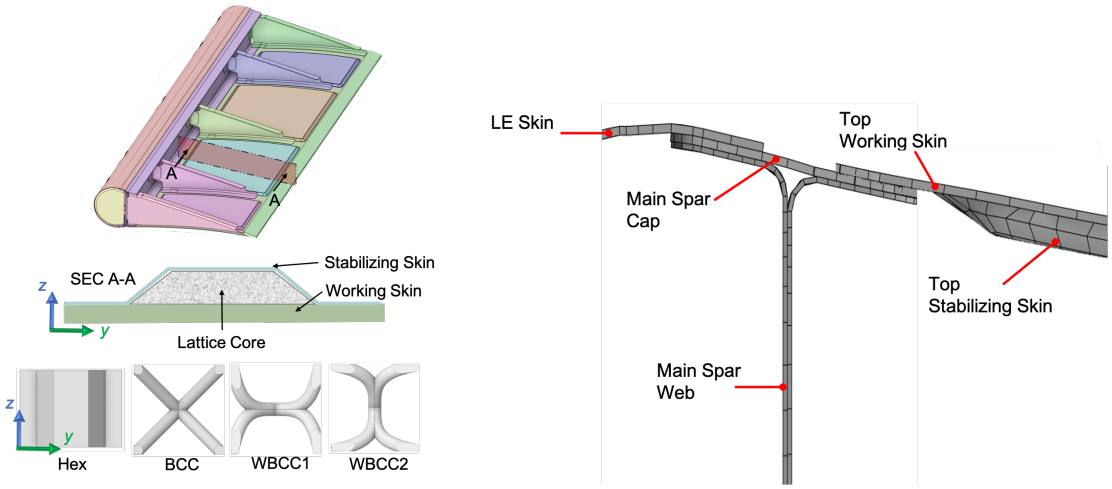

(a) (b)

Figure 5: a. Control Surface interior, asymmetric sandwich panel close-up. b. Control Surface section representation.

as an "I-section" beam, as schematically shown in Figure 5b. The laminate stacking sequence for the four mentioned components, with reference to the global coordinate system of Figure 4, is reported in Table 2.

Table 2: Laminate stacking sequence. $t_{ply} = 0.32mm$.

Top/Bottom Skin	$[(0,90)/(\pm45)/(0,90)]_s$ Working Skin	[0] Core	$[(0,90)/(\pm45)/(0,90)]$ Stabilizing Skin
Main Spar	$[(\pm45)/(0,90)]_{2s}$ Web	$[(\pm45)/(0,90)_2]_s$ Cap	
LE Skin	$[(0,90)/(\pm45)/(0,90)]_s$		

The pressure coefficient c_p acting on the control surface's outer skins was retrieved numerically using the panel method. More specifically, the open-source software XFLR5 was used to analyse the wing's airfoil first and then the behaviour of the control surface. In this early study stage, constant pressures (represented by the average c_p values, as reported in Figure 6) are uniformly applied on the upper and lower skin surfaces.

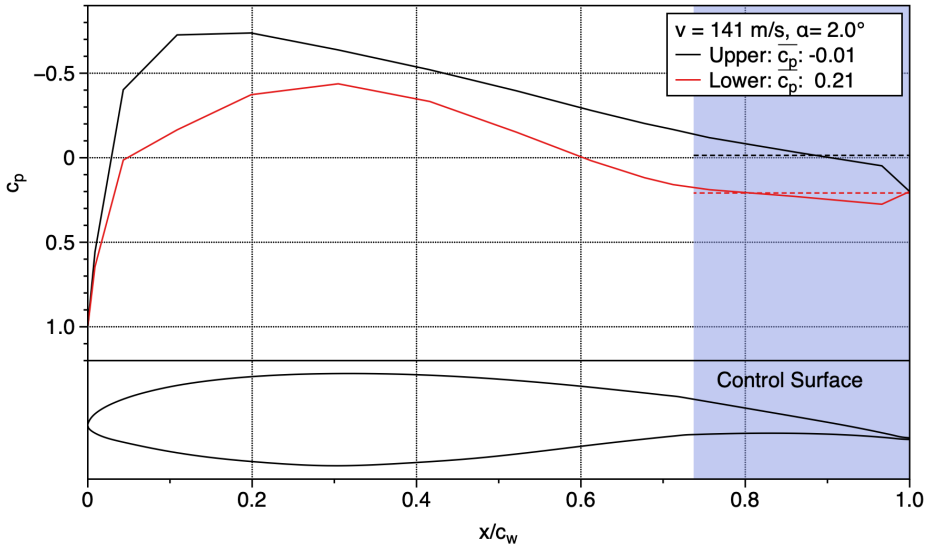

Figure 6: Variation of the pressure coefficient c_p as a function of the normalised wing's chord position x/c_{wing}. Mean values on the control surface's upper and lower skins.

DOI: 10.13009/EUCASS2023-090

As depicted in Figure 4, five hinges connect the control surface to the main wing, allowing the surface to be deflected. Therefore, the boundary conditions are completed by imposing displacement constraints on the hinge surfaces, represented by the yellow surfaces in Figure 7 Right. The displacement constraints are defined with respect to the two cylindrical coordinate systems depicted in Figure 7 Right, where u_x, u_y, and u_z correspond to the radial, tangential, and axial displacements, respectively.

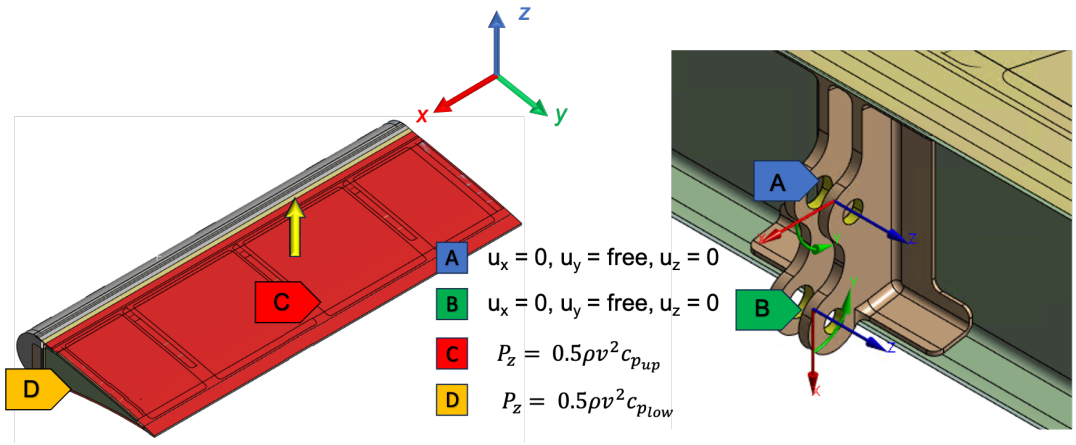

Figure 7: FEM Analyses Boundary Conditions. Left: Pressures on the upper and lower control surface skins (C & D areas). Right: Hinge detail, boundary conditions (A & B areas).

Figure 8 presents the contour map illustrating deformation along the z-direction specifically for the honeycomb configuration. As expected, the central area of the lower surface between the control surface ribs exhibits the highest degree of deformation due to the c_p values retrieved. In terms of overall deformation, no significant differences are observed among the contour maps for the remaining three core configurations. The sandwich structure experiences membrane stresses on its external skins, while the core primarily endures shear stresses as a consequence of the imposed load and boundary constraints. However, in this global analysis, the use of an equivalent homogenised core limits the extraction of relevant information regarding the core itself as the stresses would lack physical meaning. Consequently, the results focus on the displacements along the z-direction to compare the overall rigidity of the structure.

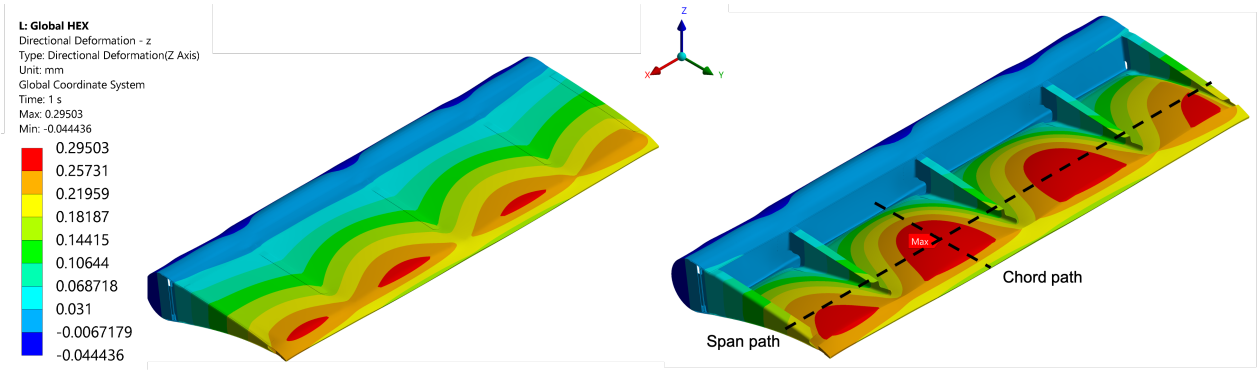

Figure 8: Directional deformation z-direction [mm]. Left: Whole structure. Right: Maximum deflection on lower skin detail.

Figures 9 and 10 compare the directional deformation along the z-direction for the upper and lower skins of the four examined lattice cores as a function of the control surface chord and span, respectively. In both cases, the honeycomb core experiences the lowest deformation resulting in a stiffer structure than the other lattice cores, while the WBCC1 experiences the highest deformations. As evidenced in Figures 9 and 10, the four suggested core topologies are equivalent for the z-directional deformation as a function of the chord on the upper skin due to the low c_p value retrieved on the upper skin. On the contrary, a maximum difference of 7% is measured between the hex and WBCC1 configurations on both the directional deformations along the chord and the span for the bottom skin.
From the WBCC1 and WBCC2 curves, it is interesting noticing that the cell orientation modifies the rigidity of the structure, thus suggesting the possibility of tailoring the overall behaviour of the structure. Rotating the WBCC cell so

DOI: 10.13009/EUCASS2023-090

that its 3^{rd} direction is aligned with the control surface's chord reduces the stiffness perpendicular to the skin. However, due to the imposed load, this is not relevant to the overall rigidity of the structure as the core withstands mainly shear deformations γ_{yz} and γ_{xz}. In the WBCC1 configuration the shear moduli G_{23} and G_{13} contribute to the panel rigidity; by rotating the WBCC cell the higher shear modulus G_{12} is activated instead of G_{23}.

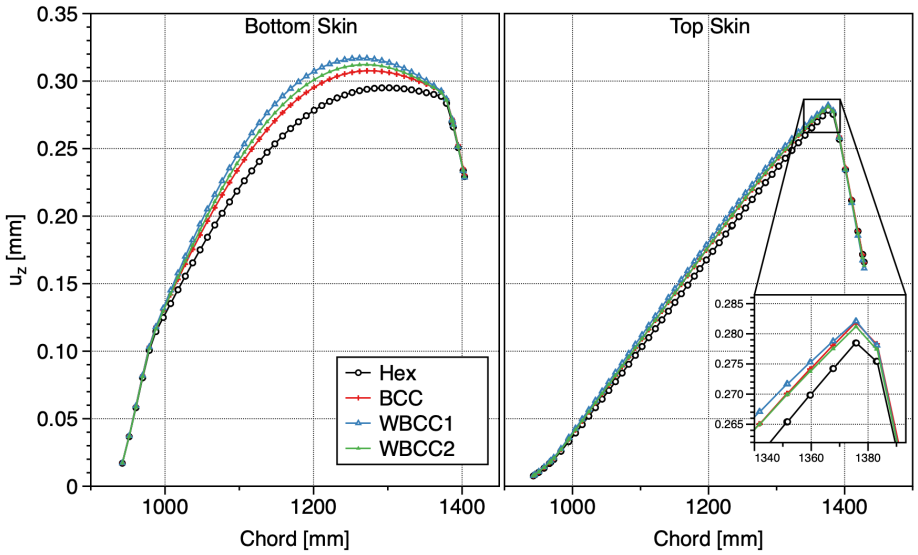

Figure 9: Comparison of the directional deformation along z-direction as a function of the control surface chord for the four lattice cores.

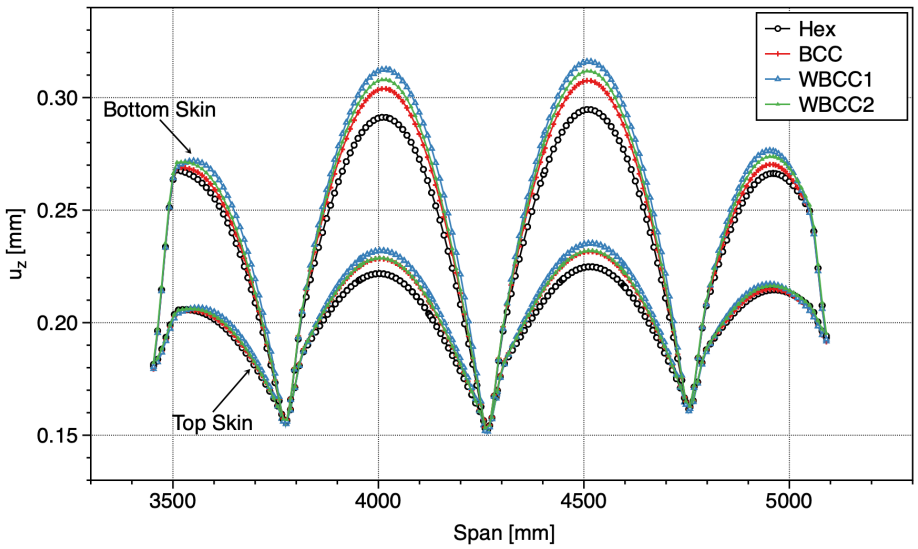

Figure 10: Comparison of the directional deformation along z-direction as a function of the control surface span for the four lattice cores.

4. Conclusions

The present paper compares the overall response of a control surface of a new-generation tiltrotor using different cores for its sandwich panels. A standard honeycomb and three strut lattice cores were analysed: Body-Centered-Cubic and a sine-Waved-Body-Centered-Cubic with two different orientations. The numerical analyses consider two-dimensional components and use homogenised cores to drastically reduce the computational effort. Since the use of the homogenised core loses information about the stresses within the core, the deflections of the whole structure were considered as a comparative means.

DOI: 10.13009/EUCASS2023-090

The findings revealed that the standard honeycomb core has the highest rigidity in contrast with the WBCC1 core configuration, which resulted in the highest deformation. However, the orientation of the unit cell is shown to influence the overall rigidity, thus giving the ability to tailor the mechanical response of the component. Furthermore, the free-form tailoring ability of additive manufacturing technologies and the ability of strut lattice components as energy absorbers or heat dissipators make these structures particularly interesting and worthy of further research.
Future investigations aim to optimise the cell performances considering different orientations and construction parameters, such as the cell size or the waviness amplitude of the struts. Through a local analysis inside the sandwich core with fully modelled cells, it would be possible to asset the stress field, thus comparing the influence of the different cores topologies on the core-skin interface and the outer skins. Furthermore, understanding the stress distribution within the sandwich structure would facilitate the design of topology-optimised structures, e.g. for iso-resistant design approaches, incorporating cells with varying geometries.

5. Acknowledgments

The study was financially supported by the Italian Ministry of University and Research - M.U.R. under the DAVYD project (P.O.N. Grant ARS01_00940).

References

[1] Howard G Allen. *Analysis and design of structural sandwich panels: the commonwealth and international library: structures and solid body mechanics division*. Elsevier, 2013.

[2] Jannik Bühring, Miguel Nuño, and Kai-Uwe Schröder. Additive manufactured sandwich structures: Mechanical characterization and usage potential in small aircraft. *Aerospace Science and Technology*, 111:106548, 2021.

[3] Jack R. Vinson. Sandwich Structures. *Applied Mechanics Reviews*, 54(3):201–214, 05 2001.

[4] Bruno Castanié, Christophe Bouvet, and Malo Ginot. Review of composite sandwich structure in aeronautic applications. *Composites Part C: Open Access*, 1:100004, 2020.

[5] Nathan Wicks and John W Hutchinson. Optimal truss plates. *International journal of solids and structures*, 38(30-31):5165–5183, 2001.

[6] Carlo Giovanni Ferro, Sara Varetti, Giorgio De Pasquale, and Paolo Maggiore. Lattice structured impact absorber with embedded anti-icing system for aircraft wings fabricated with additive SLM process. *Materials today communications*, 15:185–189, 2018.

[7] Kyohei Kohsaka, Kuniharu Ushijima, and Wesley J Cantwell. Study on vibration characteristics of sandwich beam with BCC lattice core. *Materials Science and Engineering: B*, 264:114986, 2021.

[8] Thomas Tancogne-Dejean and Dirk Mohr. Stiffness and specific energy absorption of additively-manufactured metallic BCC metamaterials composed of tapered beams. *International Journal of Mechanical Sciences*, 141:101–116, 2018.

[9] Amit Bandyopadhyay and Bryan Heer. Additive manufacturing of multi-material structures. *Materials Science and Engineering: R: Reports*, 129:1–16, 2018.

[10] Oraib Al-Ketan, Reza Rowshan, and Rashid K Abu Al-Rub. Topology-mechanical property relationship of 3D printed strut, skeletal, and sheet based periodic metallic cellular materials. *Additive Manufacturing*, 19:167–183, 2018.

[11] Davide Tumino, Andrea Alaimo, Giuseppe Mantegna, Calogero Orlando, and Stefano Valvano. Mechanical properties of BCC lattice cells with waved struts. *International Journal on Interactive Design and Manufacturing (IJIDeM)*, pages 1–14, 2023.

[12] RECEP Gümrük and RAW Mines. Compressive behaviour of stainless steel micro-lattice structures. *International Journal of Mechanical Sciences*, 68:125–139, 2013.

[13] Evangelos Ptochos and George Labeas. Elastic modulus and Poisson's ratio determination of micro-lattice cellular structures by analytical, numerical and homogenisation methods. *Journal of Sandwich Structures & Materials*, 14(5):597–626, 2012.

DOI: 10.13009/EUCASS2023-090

[14] Davide Tumino, Andrea Alaimo, Calogero Orlando, Stefano Valvano, and Carmelo Rosario Vindigni. Lattice Core FEM Simulation with a Modified-Beam Approach. In *Advances on Mechanics, Design Engineering and Manufacturing IV: Proceedings of the International Joint Conference on Mechanics, Design Engineering & Advanced Manufacturing, JCM 2022, June 1-3, 2022, Ischia, Italy*, pages 946–954. Springer, 2022.

[15] A Kumar, N Muthu, and R Ganesh Narayanan. Equivalent orthotropic properties of periodic honeycomb structure: strain-energy approach and homogenization. *International Journal of Mechanics and Materials in Design*, pages 1–27, 2022.

[16] Lorna J. Gibson and Michael F. Ashby. *Cellular Solids: Structure and Properties*. Cambridge Solid State Science Series. Cambridge University Press, 2 edition, 1997.